JGR Atmospheres

RESEARCH ARTICLE
10.1029/2021JD035741

Cold Air Outbreaks in Fram Strait: Climatology, Trends, and Observations During an Extreme Season in 2020

Sandro Dahlke[1], **Amélie Solbès**[2], **and Marion Maturilli**[1]

[1]Alfred Wegener Institute, Helmholtz Centre for Polar and Marine Research, Potsdam, Germany, [2]Faculty of Physics and Astronomy, Potsdam University, Potsdam, Germany

Key Points:

- 1979–2020 climatology of marine cold air outbreaks (MCAOs) in Fram Strait
- Significant MCAO increase in March is dynamically driven; significant decrease in mid-winter due to vertical distribution of warming
- Anomalous circulation in February/March 2020 yields extreme MCAO season with observed air mass preconditioning

Supporting Information:

Supporting Information may be found in the online version of this article.

Correspondence to:

S. Dahlke,
sandro.dahlke@awi.de

Citation:

Dahlke, S., Solbès, A., & Maturilli, M. (2022). Cold air outbreaks in Fram Strait: Climatology, trends, and observations during an extreme season in 2020. *Journal of Geophysical Research: Atmospheres*, *127*, e2021JD035741. https://doi.org/10.1029/2021JD035741

Received 24 AUG 2021
Accepted 20 JAN 2022

Author Contributions:

Conceptualization: Sandro Dahlke, Amélie Solbès
Formal analysis: Sandro Dahlke, Amélie Solbès
Funding acquisition: Marion Maturilli
Investigation: Amélie Solbès
Methodology: Sandro Dahlke
Project Administration: Marion Maturilli
Supervision: Marion Maturilli
Visualization: Sandro Dahlke
Writing – original draft: Sandro Dahlke
Writing – review & editing: Marion Maturilli

Abstract Fram Strait in the northern North Atlantic is a key region for marine cold air outbreaks (MCAOs), southward discharges of polar air under northerly air flow, which have a strong impact on air-sea heat fluxes, boundary layer processes and severe weather. This study investigates climatologies and decadal trends of Fram Strait MCAOs of different intensity classes based on the ERA5 reanalysis product for 1979–2020. Among striking interannual variability, it is shown that the main MCAO season is December through March, when MCAOs occur around 2/3 of the time. We report on significant decadal MCAO decreases in December and January, and a significant increase in March. While the mid-winter decrease is mainly related to the different paces of warming between the surface and the lower atmosphere, the increase in March can be related to changes in synoptic circulation patterns. As an explanation for the latter, a possible feedback between retreating Barents Sea sea ice, enhanced cyclonic activity and Fram Strait MCAOs is postulated. Exemplifying the trend toward stronger MCAOs during March, the study details the recordbreaking MCAO season in early 2020, and an observational case study of an extreme MCAO event in March 2020 is conducted. Thereby, radiosonde observations are combined with kinematic air back-trajectories to provide rare observational evidence for the diabatic cooling and drying during the MCAO preconditioning phase.

1. Introduction

The polar seas in the Arctic realm play an important role for the coupled climate system. A key region for air-sea interactions and transport processes is Fram Strait, the passage between Greenland and Svalbard in the high latitude North Atlantic. Especially in the cold seasons, its open water areas are characterized by comparably high sea surface temperatures (SSTs), that are in sharp contrast to much lower temperatures over the Arctic sea ice in the north (Serreze et al., 2011). Substantial atmospheric variability is caused by large scale atmospheric circulation patterns, in particular via the passage of Arctic cyclones. They drive regional meridional advection, that may lead to warm and moist air intrusions from lower latitudes into the Arctic (Kim et al., 2017; Woods & Caballero, 2016). Vice versa, southward discharges of cold and dry central Arctic air across the ice edge over the open water can lead to excessive cold spells, a phenomenon referred to as MCAOs. Marine cold air outbreaks receive attention because they typically impose strong vertical temperature gradients in the lower troposphere over the Nordic seas that reduce stability, cause incisive sensible and latent energy fluxes from the ocean to the atmosphere, and can result in anomalously deep and convective boundary layers (Brümmer, 1996; Kolstad et al., 2009; Papritz & Spengler, 2017; Terpstra et al., 2021; Tetzlaff et al., 2014). A common feature arising due to the large fluxes are convective cloud rolls and cloud streets in the direction of the air flow over the open ocean (Kolstad, 2017; Tetzlaff et al., 2014), which can be easily identified in satellite images during MCAOs (Figure 1). While the marginal sea ice zone in general has been identified as a key region of cyclogenesis (Inoue & Hori, 2011), the occurrence of MCAOs, given their imprint on local baroclinicity, has furthermore been linked to the generation of polar mesoscale cyclones and polar lows. The latter are particularly small scale and intense cyclones with a life time of only 1–2 days (Landgren et al., 2019; Meyer et al., 2021; Stoll et al., 2018; Terpstra et al., 2021). See Meyer et al. (2021) for a thorough review on the association between polar lows and MCAOs. However, even if a MCAO does not develop a polar low, it can ultimately generate extreme weather conditions, such as anomalously high surface winds, strong precipitation and freezing sea spray, imposing a direct hazard to human activity in the affected region (Kolstad, 2017; Landgren et al., 2019). From an atmospheric point of view, MCAOs are key to the energy exchange and air mass transformations between the Arctic and lower latitudes, as the initially dry and cold air masses are rapidly picking up heat and moisture from the ocean, with large implications for boundary layer dynamics and cloud formation (Papritz & Spengler, 2017; Pithan et al., 2018). Papritz

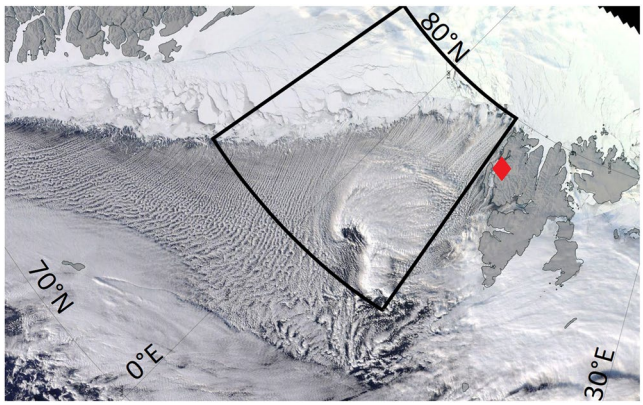

Figure 1. TERRA/MODIS satellite image of true color reflectance during a marine cold air outbreak in Fram Strait on 11 March 2020. Fram Strait box is indicated in black, and the location of Ny-Ålesund in red. Note the pronounced cloud streets due to convective roll circulations south of the ice edge. Picture modified from NASA Worldview (https://worldview.earthdata.nasa.gov/, accessed 20 May 2020).

et al. (2019) and Papritz (2020) furthermore emphasize the role of thermodynamic preconditioning of the air masses prior to the actual outbreak event, when the air is exposed to continuous diabatic cooling in the inner Arctic.

Marine cold air outbreaks typically last for only a few days (Terpstra et al., 2021), but they can in some cases prevail as long as 50 days depending on their individual definition (Kolstad, 2017). On account of the characteristical strong vertical temperature gradients involved, most studies on MCAOs have used vertical potential temperature differences between the (sea) surface and the lower to mid troposphere as a measure for MCAO detection. Given that the amplitude of synoptic temperature variability in tropospheric levels is generally much larger and occurs on shorter time scales than SST fluctuations, MCAO variability is primarily governed by the troposphere. On the other hand, SSTs shape the MCAO seasonal cycle (Kolstad et al., 2009) and SST anomalies have been shown to precede MCAOs in the Barents Sea (Polkova et al., 2021). From an oceanic point of view, MCAOs have a large effect on heat extraction from the mixed layer and related SST cooling, which can affect deep water formation in the Nordic seas and ultimately even the thermohaline circulation (Dickson et al., 1996; Isachsen et al., 2013; Papritz & Spengler, 2017; Terpstra et al., 2021). Furthermore, the West Spitsbergen Current (WSC) carries warm and saline Atlantic water northward through Fram Strait, where it strongly shapes the surface climate in the broader Svalbard region and additionally drives sea ice melt processes north of it (Duarte et al., 2020; Walczowski & Piechura, 2011). Cokelet et al. (2008) estimated that the WSC is exposed to heat loss of 200–500 W m^{-2} along its path, and the bulk of that is taken up by the much colder atmosphere. In that context, Papritz and Spengler (2017) more generally concluded that 60%–80% of the winter time oceanic heat loss in the Nordic Seas is due to MCAOs. In summary, MCAOs are important for a variety of processes and feedbacks in the Arctic climate system, involving the atmosphere, the ocean and the cryosphere. Much work has been done on characterizing North Atlantic MCAOs and their associated impact on weather and climate. On the other hand, little attention has been brought to potential long-term changes in Fram Strait MCAOs and their causes and implications, despite the fact that the North Atlantic sector of the Arctic has been identified as a key region of recent climate change with regards to observed warming, circulation changes and sea ice retreat. Additionally, most MCAO studies are essentially built on long-term, gridded data sets, such as atmospheric reanalysis products. In situ observations of MCAO events however remain sparse and difficult to obtain, especially those capturing the air mass preconditioning process, and the associated vertical structure of the atmospheric column. In an account on those points, this study investigates the climatology and decadal trends of Fram Strait MCAOs based on reanalysis data, and an analysis of potential drivers of the latter is presented. As an example consistent with the MCAO increase identified for March, a case study is conducted for the extreme MCAO season in early 2020, including observations of the air mass preconditioning and its impact on the vertical column during an extreme MCAO case.

2. Data

2.1. ERA5 Atmospheric Reanalysis

For the MCAO calculation and associated circulation features we use daily fields of temperature, skin temperature, surface pressure and mean sea level pressure (MSLP) from the novel ECMWF ERA5 reanalysis product (Hersbach et al., 2020). It was shown that over the Arctic sea ice ERA5 has, much like other state of the art reanalyses, marked biases with regard to (near) surface temperature, as well as turbulent heat and radiative fluxes, especially in winter (Graham, Cohen, et al., 2019; Wang et al., 2019). However, in comparison with observational data, ERA5 shows a remarkably good temporal correlation even in winter for most near-surface meteorological parameters (Graham, Cohen, et al., 2019). Moreover, ERA5 has been shown to outperform other reanalyses with respect to wind and temperature fields over the relatively warm waters in the Fram Strait region (Graham, Hudson, & Maturilli, 2019), which are most relevant for this study.

2.2. Sea Ice Concentration and North Atlantic Oscillation

For the analysis of drivers of MCAO variability, estimates of sea ice concentration (SIC) and the North Atlantic Oscillation (NAO) are studied for the 1979–2020 period. For SIC, the Met Office Hadley Center's monthly mean product (HadISST, Rayner et al., 2003) at 1° spatial resolution is employed. Regarding the NAO, we use the monthly mean index provided by NOAA (National Oceanic and Atmospheric Administration, https://www.ncdc.noaa.gov/teleconnections/nao/), which is derived from rotated empirical orthogonal function analysis of the 500 hPa geopotential height fields in the northern hemisphere.

2.3. HYSPLIT Trajectory Model

Thermodynamic properties along a NOAA The Hybrid Single-Particle Lagrangian Integrated Trajectory (HYSPLIT) air back-trajectory are utilized for an exemplary MCAO case in 2020. The trajectory data were retrieved from the READY web version of HYSPLIT (Rolph et al., 2017; Stein et al., 2015). As meteorological input field, the NCEP Global Forecast System (GFS) data at 0.25° horizontal resolution were chosen. Vertical movements were allowed according to the model vertical velocity.

2.4. Radiosondes

Vertical profiles of temperature and humidity from routinely launched radiosondes have been utilized for both the Arctic research station Ny-Ålesund (Maturilli et al., 2020) and for the research icebreaker Polarstern during the MOSAiC expedition 2019/2020 in the Central Arctic Ocean (Alfred-Wegener-Institut Helmholtz-Zentrum für Polar-und Meeresforschung (2017); Maturilli et al., 2021). Soundings at both locations have been conducted using Vaisala RS41 radiosondes, and specific humidity was calculated after Hyland and Wexler (1983).

3. Methods

3.1. MCAO Classification

Marine cold air outbreaks are characterized by marked vertical potential temperature gradients between the lower troposphere and the surface. In this study we construct a daily MCAO-index M which is area-averaged in a Fram Strait box (75°N–80°N, 10°W–10°E, see box in Figure 1), and which consists of $M = \theta_{SKT}–\theta_{850}$, where θ_{SKT} is the potential skin temperature and θ_{850} is the potential temperature at 850 hPa. Potential temperature is defined as

$$\theta = T\left(\frac{p_0}{p}\right)^{R/c_p}$$

with $p_0 = 1000$ hPa and $R/c_p = 0.286$. Skin temperatures over sea ice are seasonally very different from those over open water, and are used to identify ice cover. Grid boxes are assumed to be ice-covered and excluded from the area-averaging if their skin temperatures are below 271.5 K between September and April, or below 274.15 K between May through August. This step ensures to focus the analysis more on the open water areas in the Fram Strait, and we note that the main qualitative results are not sensitive to reasonable variations in those numbers. As soon as M turnes positive on a particular day, an MCAO event starts, and the end of the event is given by the first day when M turnes negative afterward. In accordance with other studies (Knudsen et al., 2018; Vavrus et al., 2006) it is required that an MCAO event lasts at least two consecutive time steps to filter out single day events that can be forced by local radiative effects, although this may be more relevant for continental cold air outbreaks. Within an identified event, we distinguish daily MCAOs of different strength, including weak ($M < 4$ K), moderate (4K $< M <$ 8 K), strong (8 K $< M <$ 12 K) and very strong ($M >$ 12 K) ones. These classes are consistent with the ones used in Papritz and Spengler (2017).

We chose the 850 hPa level for MCAO identification. Across the literature (Kolstad et al., 2009; Kolstad, 2017; Kolstad & Bracegirdle, 2008; Knudsen et al., 2018; Landgren et al., 2019; Papritz et al., 2019), typical pressure levels chosen for the lower troposphere range between 900, 850, 700, 500 hPa and a more dynamical formulation in the Lagrangian approach of Papritz and Spengler (2017). The usage of the 700 or even 500 hPa level as the upper bound for the MCAO identification criterion can be justified in cases when the MCAOs shall be related to polar lows, as those are typically identified at 500 hPa (Landgren et al., 2019), and the usage of 500 hPa can

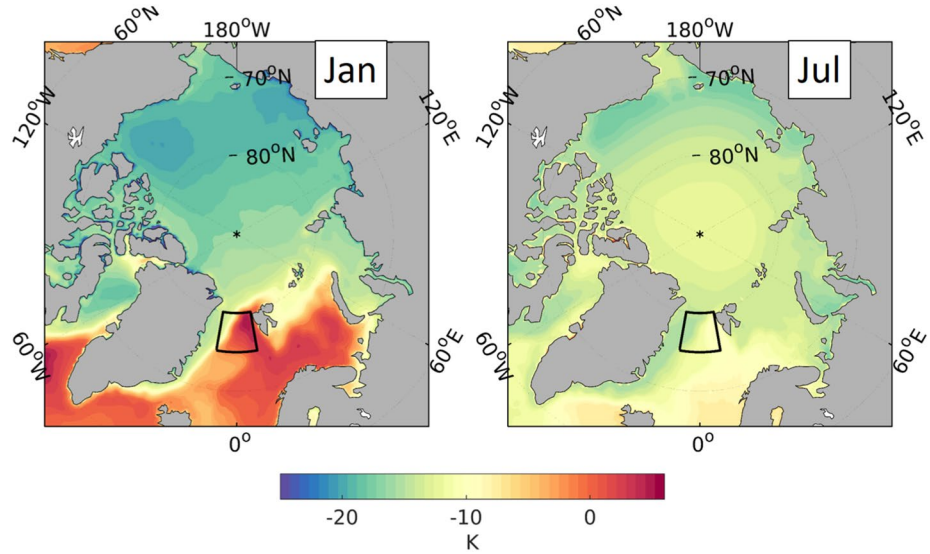

Figure 2. Monthly mean θ_{SKT}–θ_{850} difference, averaged 1979–2020 for January (left) and July (right). The full annual cycle can be seen in Figure S1.

be more powerful in filtering out non-polar low cases (Stoll et al., 2018). On the other hand it is argued that altitudes such as 500 hPa may be too far elevated to still capture the typical vertical thermal gradients that govern the boundary layer during MCAOs (Bracegirdle & Gray, 2008). Figure 2 shows the 1979–2020 climatological vertical gradients of potential temperature for two months representative for the cold and warm season. The full annual cycle can be seen in Figure S1. Regions of enhanced positive values can be interpreteted as potential hot spots for MCAOs. The regional patterns are consistent with earlier studies (Kolstad et al., 2009; Papritz & Spengler, 2017), who showed that the largest potential for MCAOs is from early winter to spring over the comparably warm open water areas of the North Atlantic and Barents Sea. Thereby, the Fram Strait region west of Svalbard and the western Barents Sea appear to be MCAO key regions, which was also found in Kolstad et al. (2008) and Terpstra et al. (2021).

3.2. Trend Calculation

In this study, trends are estimated with the Theil-Sen trend estimator (Sen, 1968; Theil, 1950). This is a non-parametric test that is independent of the statistical distribution of the sample data, and is in comparison to a least squares fit less susceptible to potential outliers or extremes, yielding robust trend estimates for hydrological and climate time series (Yue et al., 2002). Significant autocorrelation in a timeseries reduces the number of degrees of freedom and hence impacts the significance level of a derived trend. On account of reducing such potential impacts, we follow the trend-free prewhitening procedure of Yue et al. (2002), that is outlined in the following. The Theil-Sen trend slope m is first removed from the time series $Y(t)$ by introducing the anomaly time series

$$Y'(t) = Y(t) - m \cdot t.$$

If a significant (95%) lag 1 autocorrelation is detected in Y', the serially correlated part is subtracted by the prewhitening:

$$Y''(t) = Y'(t) - r_1 Y'(t-1).$$

where r_1 is the lag-1 autocorrelation coefficient of Y'. Finally, the prewhitened series and the trend are blended again by letting

$$Y^*(t) = Y''(t) + m \cdot t.$$

By doing so, the effect of autocorrelation is removed, while Y^* still preserves the original trend and remaining variability of the time series. Finally, the non-parametric Mann-Kendall test (Kendall, 1975; Mann, 1945) is

applied to Y^* to test whether the trend is significant (95%). In case no significant autocorrelation was initially detected in Y', the last two steps are skipped and the Mann-Kendall test is applied directly to Y. We note however that in fact none of the trends that are discussed in this study are found to be autotocorrelated, hence this procedure does not affect the conclusions. 95% confidence bounds are estimated using the non-parametric approach of Sen (1968).

3.3. Composite Analysis

Section 4.4.2 presents composite anomalies for "low SIC minus high SIC" and "high MCAO minus low MCAO" conditions. As an example for the latter case, these composites reflect the average difference between the 10 years of highest monthly mean M minus the 10 years of lowest monthly mean M. On a similar note, low SIC minus high SIC composites correspond to the average difference between the 10 years of lowest and highest monthly mean SIC, where SIC has prior been area-averaged in the box covering 30°E–60°E, 74°N–79°N). Note that for all composites, the time series which is subject to compositing has been detrended beforehand. With this step we aim to capture interannual maxima/minima relative to a potential overarching trend, instead of simply reproducing the latter with the composite. We note that without detrending, the results are nonetheless qualitatively similar, but the composite anomalies are stronger and more widespread. For estimating statistical significance of the composite anomalies, a Monte Carlo approach was used where the composite members were randomly drawn from the 1979–2020 period. This resampling was repeated 10,000 times and the resulting Monte Carlo composite was compared to the original decomposition using the z-statistic:

$$z = \frac{\mathrm{COMP}_{\mathrm{Orig}} - \overline{\mathrm{COMP}_{\mathrm{MC}}}}{\sigma_{\mathrm{MC}}/\sqrt{n}},$$

where $\mathrm{COMP}_{\mathrm{Orig}}$ is the original composite, $\overline{\mathrm{COMP}_{\mathrm{MC}}}$ is the averaged Monte Carlo composite, σ_{MC} its standard deviation, and n is the number of composite members (10).

4. Results

4.1. Fram Strait MCAO Climatology

We first provide a comprehensive overview on the long-term statistics of the Fram Strait MCAO index M in Figure 3a, as well as on the occurrence frequencies of MCAOs of different intensities in Figure 3b. In general, MCAOs occur from October through April, and a strong interannual variability can be seen in both the daily index itself and in the occurrence frequencies of all MCAO intensity classes. During the extended winter period (November through March), weak MCAOs ($M > 2$ K) typically occur at 20%–25% of the time, and in individual years they may occur more often than 40% of the time, or less often than 10% of the time (Figure 3b). The results show that stronger MCAOs are generally less frequent than weaker ones. Very strong ($M > 12$ K) MCAOs typically occur at 5%–10% of the time, and may occur up to 20% of the time, or not at all in some years. Note that these occurrence frequencies are additive between the intensity classes, so MCAOs prevail around 2/3 of the time and the numbers agree well with the estimates in Papritz and Spengler (2017), who found typical frequencies of MCAOs exceeding 12 K in intensity of the order of 5%–9% in Fram Strait. Their study also revealed that the vast majority of the strongest MCAOs in the Nordic Seas take place over the open waters of eastern Fram Strait, west of the Svalbard archipelago, further pinpointing this region as a hot spot of particularly strong MCAOs. It should be noted however that these events are nonetheless quite rare, as the average MCAO index from December through March is between 2.8 and 3.1 K (Figure 3a). From June to August, MCAOs are virtually absent, and the average MCAO index is then even negative between −5 and −11 K.

4.2. Role of Atmospheric Circulation

In this section it will be analyzed what constellation of atmospheric circulation patterns are conducive for Fram Strait MCAOs. For each month, the average daily surface pressure anomaly during the strongest 10%, 5% and 1% of MCAOs (90th,95th and 99th percentile) was calculated, and the results are shown exemplarily for January in Figure 4. A consistent picture emerges, which is qualitatively also valid for the months which are not displayed. Strongest MCAOs are associated with a dipole-like pattern, consisting of anomalous low pressure over Novaya

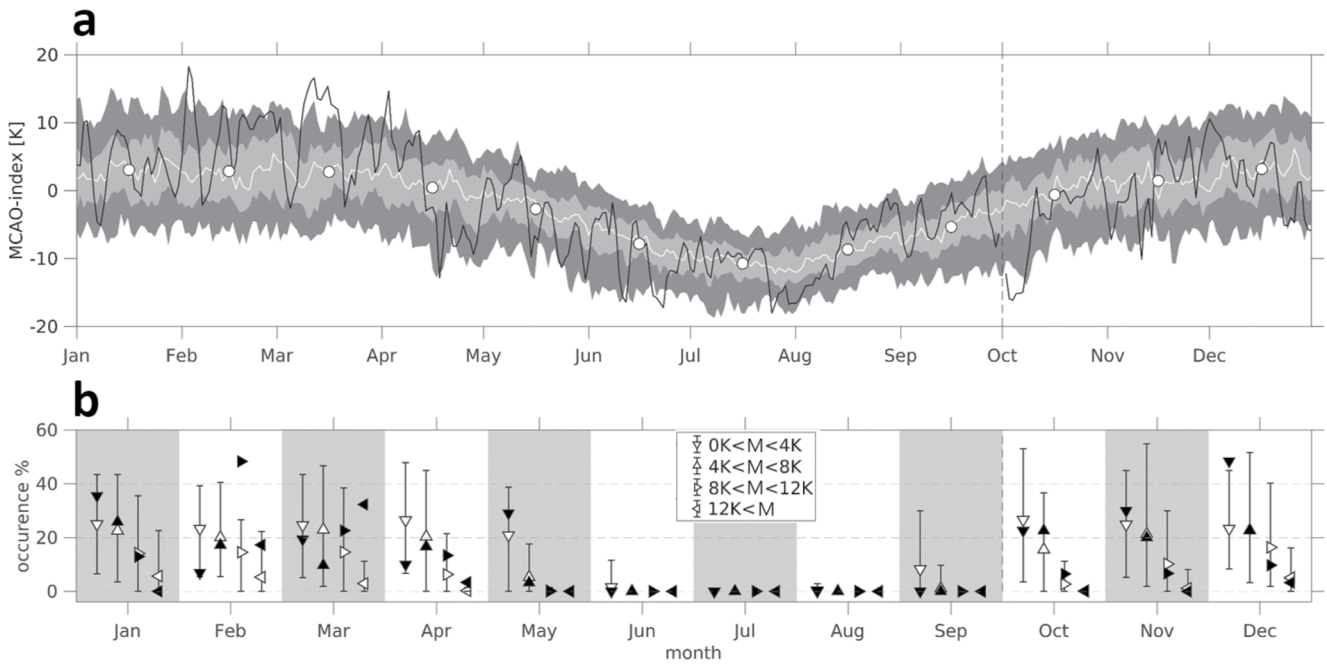

Figure 3. (a) 1979–2020 median of daily marine cold air outbreak (MCAO) index in Fram Box (white line), including 25–75 (light gray shading) and 5–95 (dark gray shading) percentiles. Black line indicates the MOSAiC year (October 2019–September 2020, separated by vertical dashed line). Monthly mean values are given as white dots. (b) Box plot of climatological occurrence frequencies of MCAOs of different intensities, including the median, 5th and 95th percentiles (white markers and whiskers), and corresponding values during the MOSAiC year (single black markers).

Zemlya and the eastern Barents Sea, and anomalous high pressure over parts of Greenland and the adjacent ocean. This anomalous dipole pattern translates to an anomalous zonal pressure gradient across Fram Strait, as indicated by the isobars. It is hence very effective in southward geostrophic advection of cold, Arctic air masses over the ice edge toward the open water areas of the Nordic Seas which is characteristic for MCAOs (Kolstad, 2017; Papritz & Spengler, 2017). The resulting patterns are qualitatively similar among the investigated MCAO intensities, but their amplitude is higher for more extreme events, which also translates to stronger zonal pressure gradients and related stronger northerlies during the more extreme MCAO cases. Hence, the MCAO intensity scales to a first

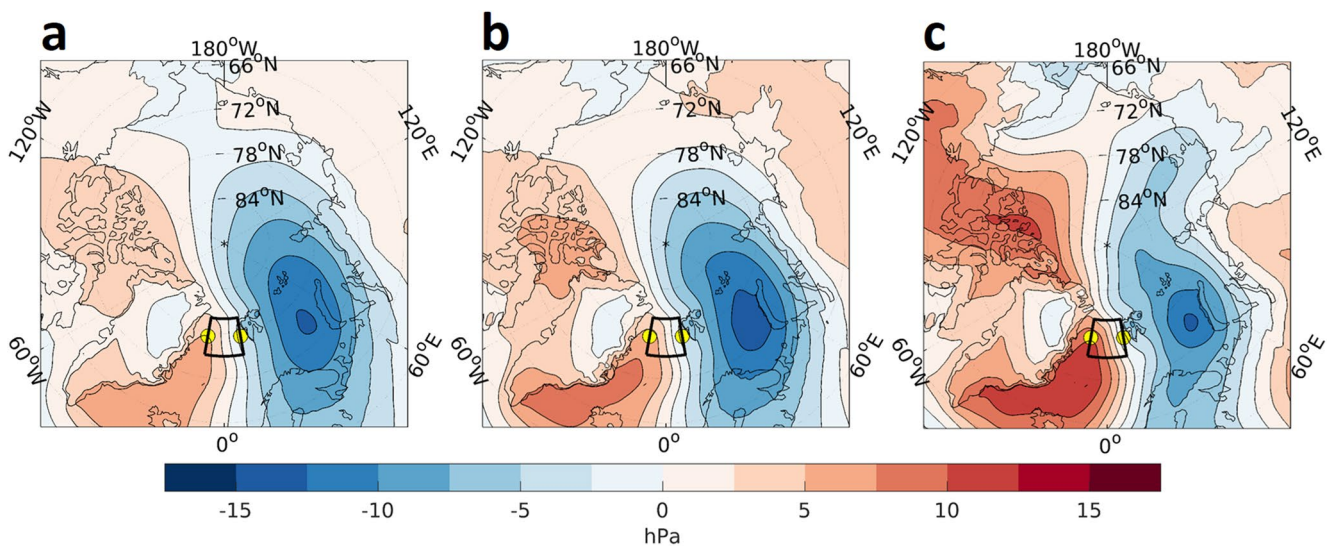

Figure 4. January surface pressure anomaly composite maps for the (a) 90th, (b) 95th and (c) 99th percentile of strongest Fram Strait marine cold air outbreaks. The Fram Strait box is indicated as bold black contour, and the cross-Fram Strait surface pressure gradient is calculated between the two yellow dots, respectively.

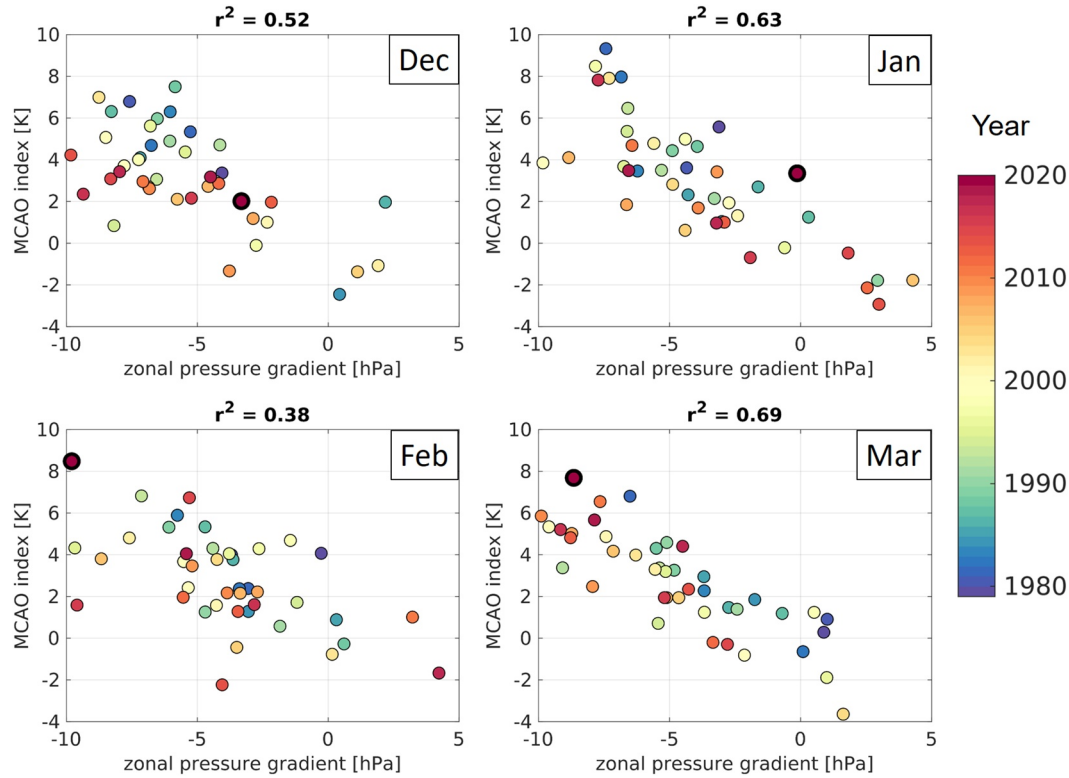

Figure 5. Scatter plots of monthly mean zonal surface pressure gradient across Fram Strait (77.5°N, 10°E minus 77.5°N, 10°W) versus monthly mean marine cold air outbreaks (MCAOs) index. Color of the dots corresponds to the year and the squared Pearson correlation coefficient of the detrended series is given in the top, respectively. The 2020 data point has been highlighted.

order with the zonal pressure gradient across Fram Strait and related meridional advection processes, implying that atmospheric dynamics play an important role in shaping interannual MCAO variability. To shed further light on this aspect, we analyzed long-term variability in the zonal pressure gradient across the Fram Strait box and related it to the monthly MCAO index. The results are shown in Figure 5 for the months December through March. Among all months, a significant co-variabilty between the zonal pressure gradient and the MCAO index is apparent, as indicated by the squared correlation coefficient r^2. The correlation is highest in March and weakest in February, with larger east-west pressure gradients leading to higher MCAO indices. This indicates that a large fraction of interannual MCAO variability can indeed be explained dynamically by the occurrence of the large scale weather patterns shown in Figure 4, using the zonal pressure gradient across Fram Strait as a proxy for the latter. Figure 5 also reveals that the 2020 MCAO season in February and March was a record-breaking one, as will be detailed in the next section.

4.3. A Year of New Records: 2020

Late winter/early spring 2020 featured an extraordinary atmospheric configuration over the Arctic, whose tropospheric part bears resemblance to the patterns in Figure 4 discussed above as being very favorable for particularly strong MCAOs. The stratospheric polar vortex was remarkably cold, strong and undisturbed, while the troposphere at the same time (January-March) was characterized by a record-breaking, persistent, positive phase of the Arctic Oscillation, with associated hemispheric-scale anomalies in surface air temperature, precipitation, circulation, and sea ice extent (Dethloff et al., 2021; Lawrence et al., 2020; Overland & Wang, 2021). The most relevant of those features for the present study was the persistent lower tropospheric circulation anomaly and its footprint in mean sea level pressure. It consisted of a widespread low pressure anomaly exceeding −10 hPa in amplitude, which occupied the eastern half of the Arctic Ocean (see Figure 5a in Lawrence et al., 2020), thus resembling our composite anomaly patterns for strong MCAOs shown in Figure 4. In fact, both February and

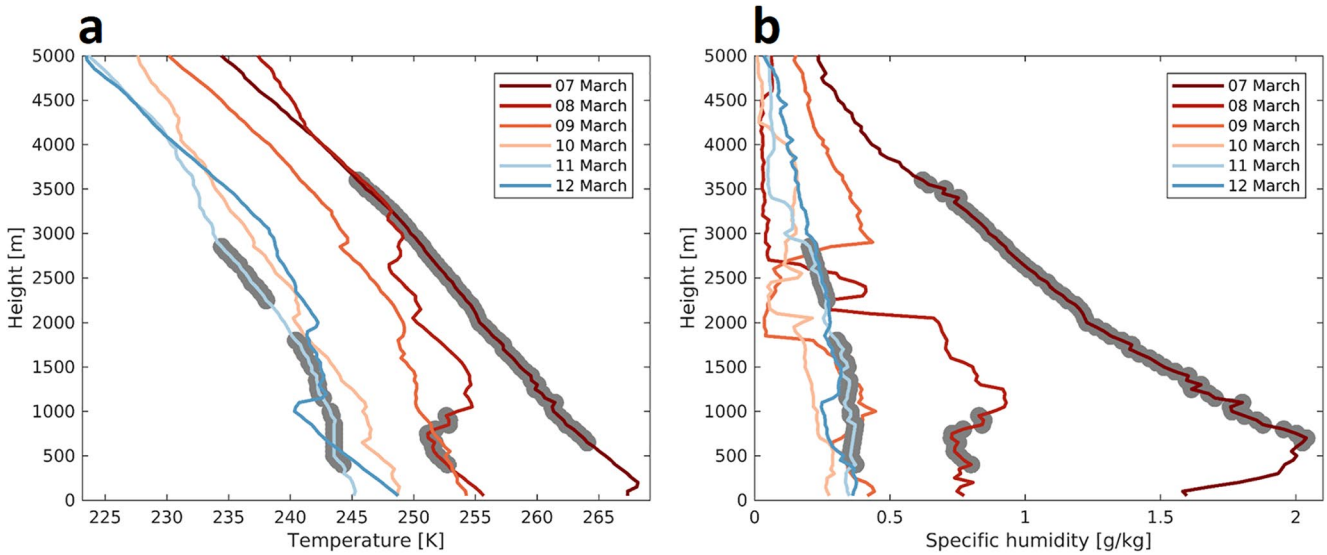

Figure 6. Vertical profiles of (a) temperature and (b) specific humidity from radiosondes in Ny-Ålesund, Svalbard, during the onset of the extreme March 2020 marine cold air outbreaks event in Fram Strait. Gray dots indicate layers where relative humidity exceeds 95%. Sondes were launched at 11 UTC on the displayed day.

March 2020 set new records for the monthly mean Fram Strait MCAO index in the ERA5 reanalysis (Figure 5), and February moreover set a new record for the cross-Fram Strait zonal pressure gradient. Figure 3 provides a more detailed view into individual events of the remarkable 2020 MCAO season. While January 2020 appears quite normal, February and March stand out as periods of unusually strong MCAOs. The daily MCAO index M in Figure 3a exceeds the 75th percentile during large parts of February and March, and even exceeds the 95th percentile during 2 individual "extreme" MCAO events. One event took place between 01 and 06 February (18.2 K peak daily intensity M) and another event during 08–20 March (16.6 K peak daily intensity M). In terms of their peak amplitude, those two events represent the strongest February event, and the second strongest March event in the whole analyzed 42 year period, respectively. Figure 3b further reveals how unprecedented the February and March 2020 MCAO situation was. Strong (February) and very strong (March) events in 2020 exceeded the 95th percentile of the climatological occurrence frequencies by a factor of 1.48 and by 2.08, respectively. To put this into climatological context, MCAO events in excess of 12 K typically occur during ~3.6% of the time in March (15.5% marks the 95th percentile), but March 2020 saw such conditions during 32.2% of the time. Hence, the persistent nature of the atmospheric circulation anomalies during late winter/early spring 2020 were clearly the drivers for the anomalous MCAO situation in Fram Strait. In the following, column observations from the Arctic during the March event are used as case study to showcase associated air mass preconditioning.

Due to the remoteness of the affected regions in the Arctic, there are typically little to no observations available for the vertical atmospheric footprint along the path of such MCAO advection events. Arctic upper air observations are generally limited to few land based research stations, like Ny-Ålesund on Svalbard (78.92°N, 11.93°E, see map in Figure 1) in close proximity to Fram Strait, where at least one radiosonde is launched per day (Maturilli & Kayser, 2017). Figure 6 shows daily tropospheric temperature and humidity profiles from the Ny-Ålesund radiosonde record during the onset of the extreme MCAO event in March 2020 in Fram Strait. Although Ny-Ålesund is located just outside the Fram Strait box for MCAO detection, the effect of advecting the MCAO-associated cold and dry air mass is clearly captured in the daily evolution. On 07 March, comparably warm and moist conditions still prevailed throughout the lower troposphere at the site, with an indication of low level clouds in the lowest few kilometers. From 08 March on, steady cooling and drying of the column can be observed throughout the troposphere, and peak minimum temperatures around (243 K) in the lowermost 1000 m are achieved around 11–12 March. Note that the extreme MCAO event in Fram Strait also began on 08 March and peaked on 12 March, which provides evidence that the column above Ny-Ålesund was affected by that particular air mass as well.

In parallel to these events, the MOSAiC campaign over the Central Arctic sea ice took place (Shupe et al., 2020). These unique observations during the 2019/2020 MCAO season are of rare nature and potentially provide

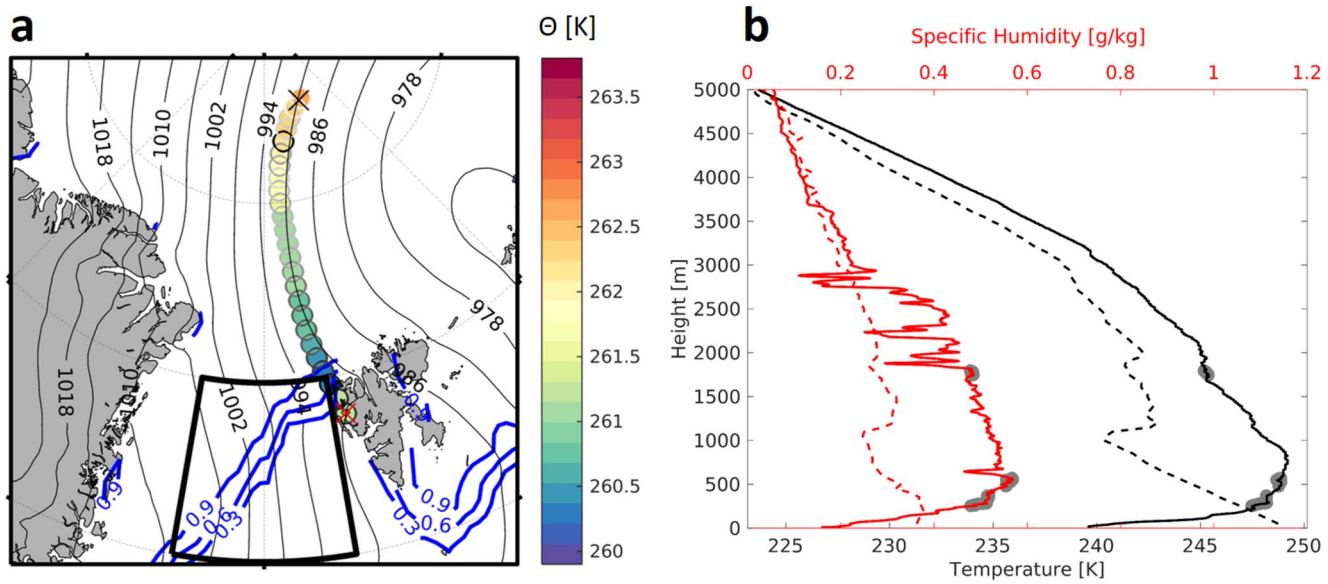

Figure 7. (a) The hybrid single-particle Lagrangian integrated trajectory 1 day air back-trajectory arriving at 1800 m height on 12 March, 11 UTC in Ny-Ålesund (78.92°N, 11.93°E, see red cross) with potential temperature along trajectory color-coded. Also shown are monthly mean sea ice concentration (HadISST, blue contours) and mean sea level pressure (black contours) on the displayed day. The location of the Polarstern icebreaker during the MOSAiC campaign on 11 March 2020, 11 UTC is indicated by a black cross (87.67°N, 24.50°E). (b) Radiosonde vertical profiles of temperature (black) and specific humidity (red) launched on 12 March 11 UTC in Ny-Ålesund (dashed line), and on 11 March 11 UTC on Polarstern (solid line). Layers with relative humidity above 95% are indicated by gray dots, respectively.

upstream information of the air mass preconditioning during the associated advection events in Fram Strait. As outlined in Kanno et al. (2015) and Messori et al. (2018), the cold and dry air in the inner Arctic can be viewed as trapped and shielded dynamically from warm and moist intrusions of lower latitudes during episodes of persistent and strong cyclonic circulation regimes in the central Arctic, being continuously exposed to diabatic cooling. Following the wording of Kanno et al. (2015), this process of "charging" the inner Arctic with cold air masses is followed by episodical "discharge" events, when that air mass is dynamically distributed to lower latitudes in the form of MCAOs. Papritz et al. (2019) and Papritz (2020) further showed that this sustained inner Arctic diabatic cooling plays an important role in generating the cold extremes that are associated with MCAOs. We adapt the methodology of Ali and Pithan (2020), who have shown that air back-trajectories can be a powerful tool connecting upper air observations from Central Arctic campaigns to corresponding observations at lower latitudes in a Lagrangian, event-matching framework. In that manner, we link Eulerian radiosonde observations from Ny-Ålesund with MOSAiC during the extreme MCAO event in March 2020 with HYSPLIT Lagrangian trajectories. We found a match between the two sites on 11–12 March, interestingly coinciding with the day of peak MCAO intensity in Fram Strait. Figure 7a shows that an airmass passing Ny-Ålesund on 12 March 11 UTC at 1800 m height had crossed the MOSAiC site 24 hr earlier. The diabatic cooling along the advection path can be seen in Figure 7a, along with the characteristic circulation pattern. Figure 7b shows the respective atmospheric temperature and humidity profiles at the MOSAiC site and in Ny-Ålesund, that correspond to the start and end points of the trajectory shown in Figure 7a. Although the MOSAiC site was located further north in the Central Arctic, both temperature and humidity above 300 m height at the site were consistently higher than one day later at Ny-Ålesund, indicating the cooling and drying of the air mass over the Arctic sea ice. Regarding the column above 1000 m height, the cooling and drying of the air mass appears to be generally stronger at lower altitudes. Note especially the good agreement of the low specific humidity estimates above 3,000 m height between the profiles, while the drying is centered below where there are still some indications for cloud occurrence during MOSAiC. While Lagrangian processes such as precipitation, cloud dissipation and radiative cooling are potential drivers for this transformation, local effects also play an important role, particularly close to the surface and in the boundary layer. For instance, the profile at MOSAiC shows the expected strong temperature inversion over sea ice of almost 10 K in the lowermost 500 m, while the profile above Ny-Ålesund shows decreasing temperature and humidity up to 1000 m height. These near surface discrepancies are difficult to interprete given the special setting of Ny-Ålesund in the interior of Kongsfjorden. As an example, the Ny-Ålesund soundings for 12 March reveal notable

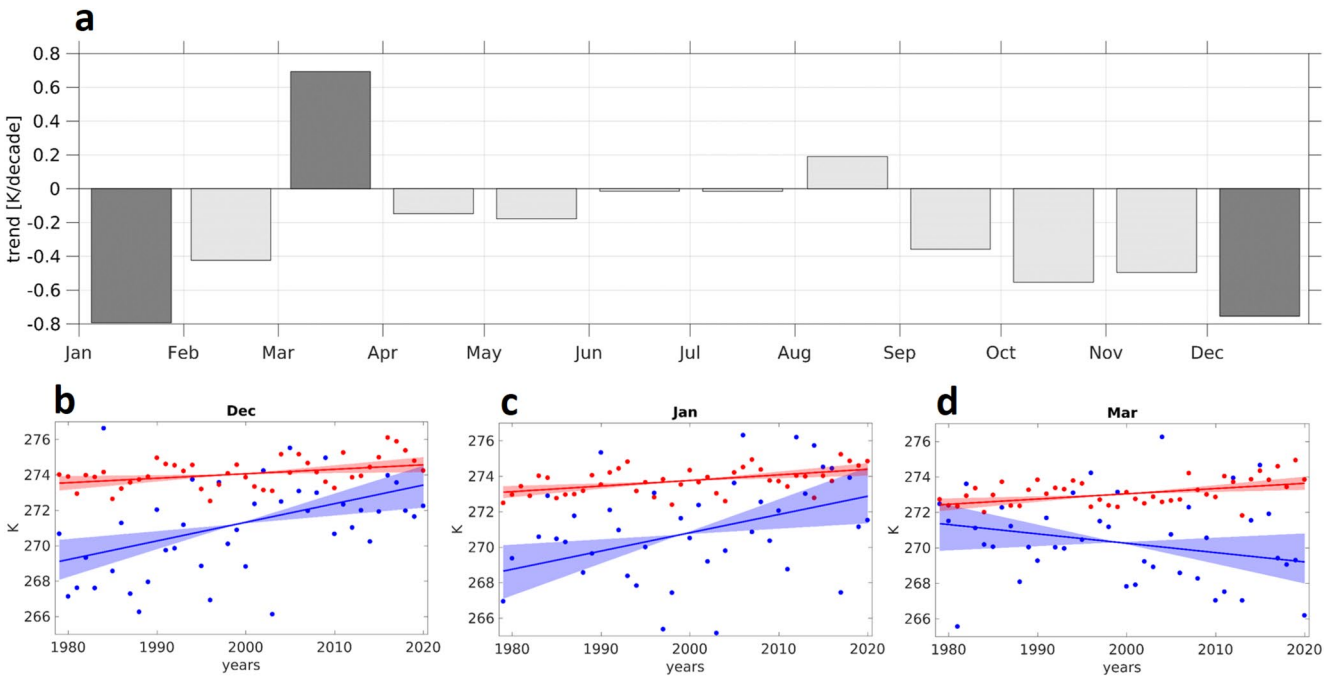

Figure 8. (a) Decadal trends of the monthly mean marine cold air outbreak index from ERA5. Statistically significant (95%) trends are indicated in dark gray. The lower panels show monthly mean Θ_{850} (blue) and Θ_{SKT} (red) area-averaged in the Fram Strait box for (b) December, (c) January, (d) March, along with their respective trends and uncertainties (95%).

average winds of 14 m s^{-1} in the lowermost 1000 m, and a consistent NW wind direction (not shown). Under such forcing, the ballon gets rapidly transported toward the nearby Zeppelin mountain and the glaciers that surround it, where surface- and lower atmospheric conditions can differ drastically from the balloon launch platform in the village. For this reason, Dahlke and Maturilli (2017) suggested that the lowermost 1000 m should be treated with much care in studies focusing on on aspects of large scale synoptic transport at the site. By putting together the essence of Figures 6 and 7 it is nonetheless intriguing that air mass transformations in association with MCAOs, and their vertical structure can be studied by means of combining in situ observations and kinematic trajectories in an event-based manner. We suggest this approach has a large potential for dedicated studies on the air mass transformation processes in association with MCAOs.

4.4. MCAO Decadal Trends and Their Causes

Given their severity and profound impacts, the question arises whether such extreme MCAO events as observed during spring 2020 are in recent years more likely to occur based on any existing trends. Here we present an analysis of long-term changes in the MCAO season and discuss their potential drivers. Figure 8a shows 1979–2020 decadal trends in the MCAO index *M* for each month. We find significant MCAO downward trends in December (−0.75 K/decade) and January (−0.79 K/decade), and surprisingly a significant increase in March (+0.69 K/decade) over the investigated period. We are not aware of any study that ever reported on significant MCAO trends in the investigated region. Kolstad et al. (2009) analyzed MCAOs in different sub-regions of the high latitude North Atlantic based on the NCEP/NCAR reanalysis, and found no significant trends in any region during the 1958–2007 period. The downward trends during winter are somewhat expected however, because strongest Arctic winter warming is observed at the (near) surface levels and in the lower troposphere (Graversen et al., 2008; Serreze et al., 2009). This also holds for Fram Strait (Dahlke et al., 2020). On the other hand, MCAO-related surface skin temperature is closely tied to the SST. Since the lower atmosphere has a much smaller heat capacity than the upper ocean layer, one would expect that the ongoing warming happens at a faster rate in the atmosphere than at the ocean surface. This argumentation is consistent with future projections in the modeling work of Landgren et al. (2019), which revealed systematic decreases in their 2006–2080 winter MCAO index over the Nordic Seas under the RCP8.5 emission scenario. This argumentation is in line with our confrontation of the warming trends

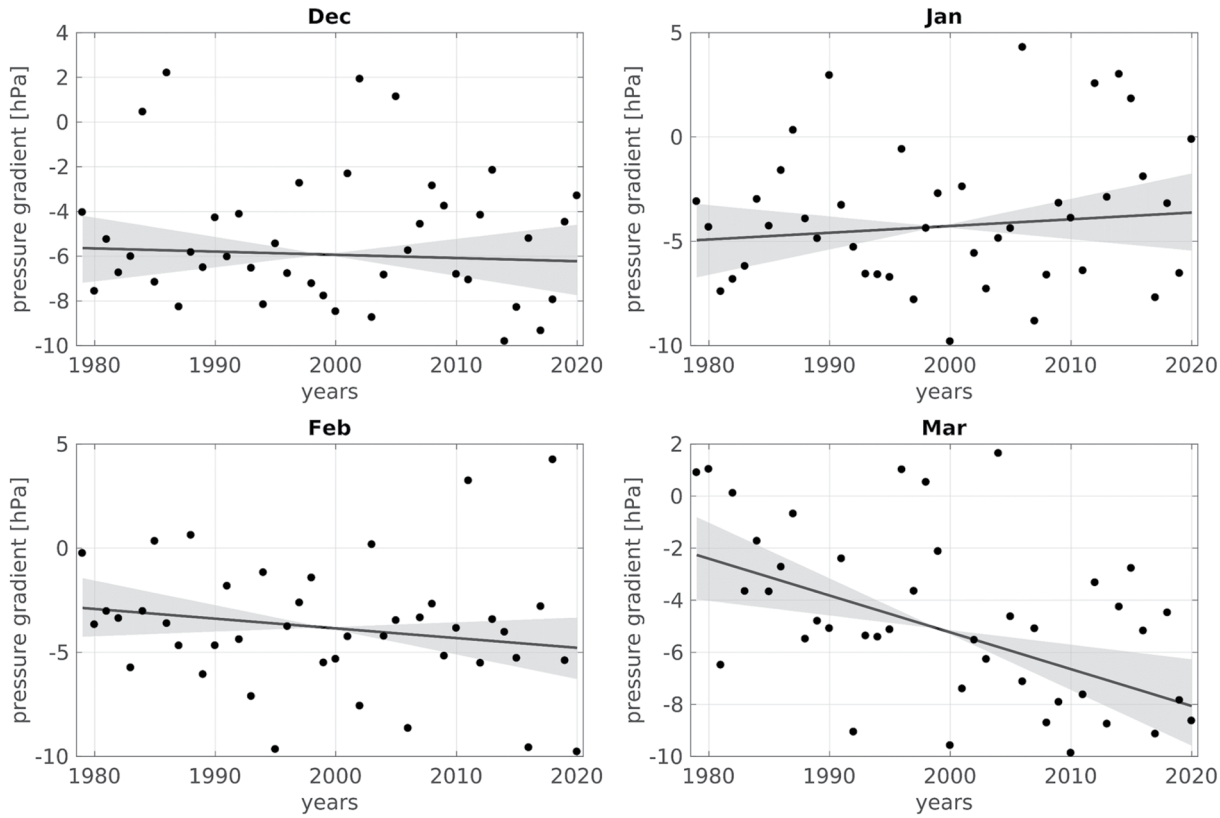

Figure 9. Zonal surface pressure gradient across the Fram Strait box (10°E, 77.5°N minus 10°W, 77.5°N, black dots) for December (top left), January (top right), February (bottom left) and March (bottom right). Linear trend using the Theil-Sen slope is indicated as black line with gray shaded confidence intervals (95%).

of Θ_{850} and Θ_{SKT} for December and January, as shown in Figures 8b and 8c, respectively. The rate of warming in Θ_{850} outpaces the one in Θ_{SKT}, which is consistent with the decreases in the MCAO index. The situation for March looks different (Figure 8d). While Θ_{SKT} is also warming in March, Θ_{850} rather has a cooling tendency (although not statistically significant at pvalue = 0.16). The lack of lower-tropospheric warming is what determines the MCAO increase in March. Next we investigate if circulation changes over Fram Strait can be used to explain these trends. Figure 9 shows monthly time series and associated trends of the cross-Fram Strait pressure gradient which was introduced in Section 4.2. March shows a significant decrease of −1.41 hPa/decade, with larger negative zonal pressure gradients in later years and weaker ones in earlier years. It is consistent with stronger/more frequent northerlies and may provide a dynamical explanation for the observed MCAO increase during March. On the other hand, the zonal cross-Fram Strait pressure gradient exhibits no significant trends in December and January, when we found a decrease in the MCAO index (Figure 8a). These results let us conclude that the MCAO decrease in mid-winter is primarily driven by the vertically differing pace of the warming between the surface and the lower atmosphere, while the observed MCAO increase in March is primarily related to changes in atmospheric dynamics. It should be noted however that atmospheric circulation changes during winter may have contributed to the overall warming in the North Atlantic sector of the Arctic by means of heat and latent energy advection (Dahlke & Maturilli, 2017; Rydsaa et al., 2021; Woods & Caballero, 2016).

What particular changes in large scale weather patterns are responsible for the identified trends in the cross-Fram Strait pressure gradient and, hence, MCAOs? We therefore investigate the relative roles of long term changes in the Barents Sea low pressure anomaly versus the Iceland/Greenland Sea high pressure anomaly (referring to the dipole pattern in Figure 4). Regional trends of 1979–2020 MSLP are provided in Figure 10. Consistent with our previous results, we find no significant changes for January through February in the displayed region. Although insignificant, December and January hint toward a negative Arctic Dipole tendency (Wu et al., 2006), as indicated by positive MSLP tendencies over Novaya Zemlya and negative MSLP anomalies over the Greenland Sea. The most striking feature of this analysis is the widespread cyclonic circulation trend over the Barents Sea in March,

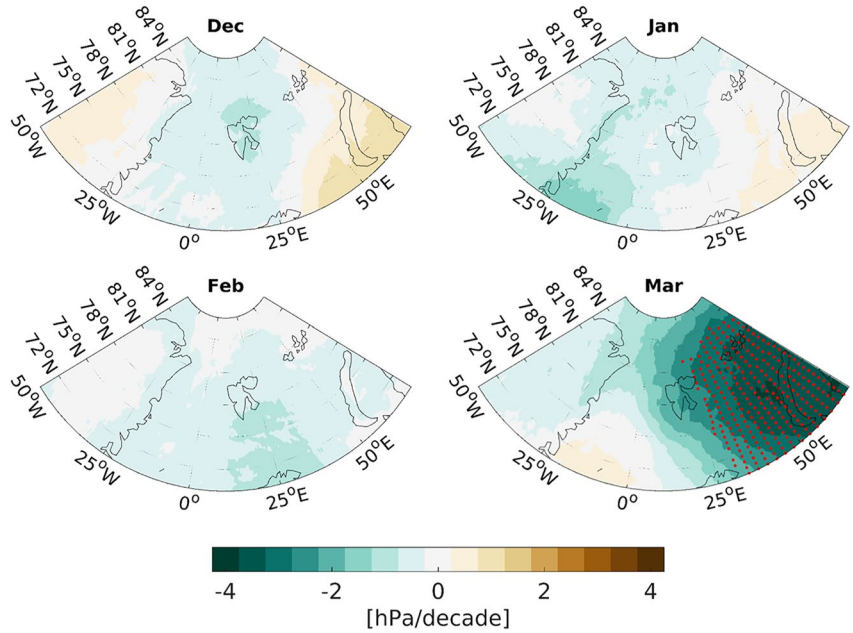

Figure 10. 1979–2020 decadal trends in mean sea level pressure for December (top left), January (top right), February (bottom left), and March (bottom right). Red dots indicate grid points with statistically significant trends (95%).

which projects onto the MCAO-related circulation pattern there (Figure 4). This suggests that Fram Strait MCAOs in March have been affected by circulation shifts centered in the Barents Sea rather than in the Greenland Sea itself. In the following, the role of SIC variability and the North Atlantic Oscillation as potential drivers for the Barents Sea circulation anomaly and the related MCAO trends are investigated.

4.4.1. Role of the North Atlantic Oscillation

The North Atlantic Oscillation (NAO) is one of the most dominant patterns of internal atmospheric variability in the northern hemisphere, and has far-reaching impacts on surface temperature, precipitation, storm tracks and more (Hurrel et al., 2003). It can be described as the dipole in MSLP anomalies between the Icelandic low and the Azores high, and it strongly determines the zonal flow across the north Atlantic. For the Norwegian Sea, Mallet et al. (2013) found that polar low outbreaks, which are closely related to MCAOs, occur twice as frequent under NAO^- conditions than under NAO^+ conditions. Hurrell et al. (2003) noted a northerly near surface wind anomaly over Fram Strait when comparing NAO^+ minus NAO^- conditions, which motivates a potential impact on MCAOs there. A correlation of the detrended monthly NAO index with the monthly MCAO index however reveals only weak correspondence of $r = 0.20$, -0.18, -0.07, and -0.26 for December, January, February and March, respectively. None of those correlations are significant. Moreover, in none of these months, the NAO index shows a significant trend (not shown) unlike the MCAO index. The low correspondence between the MCAOs and the NAO is overall not surprising, because the NAO essentially describes a zonal circulation regime, as noted above, while our results and Afargan-Gerstman et al. (2020) demonstrated that MCAOs are associated with meridional circulation regimes. This is consistent with Winther et al. (2002) who found that precipitation and temperature on Svalbard next to Fram Strait are unrelated to the NAO. Nonetheless, the Greenland Sea high pressure anomaly for MCAOs shown in Figure 4 projects on a weakened Icelandic low and hence a negative phase of the NAO, while the cyclonic Barents Sea circulation anomaly is not associated with the typical NAO pattern (Hurrell et al., 2003).

4.4.2. Role of Sea Ice Cover

It is striking that the Barents Sea cyclonic circulation anomaly from Figures 4 and 10 (March) are centered over the region of strongest seasonal sea ice loss (Onarheim et al., 2014, 2018), implying a possible connection. We here analyze the association of Fram Strait MCAOs with regional SIC anomalies in the Greenland- and Barents Sea. Figure 11 shows maps of SIC composite anomalies for "high MCAO" minus "low MCAO" conditions for December through March. See Section 3.3 for details on the definition. Across all months, MCAOs are associated with positive SIC anomalies around the Svalbard archipelago, especially in Whalers Bay north of it, which

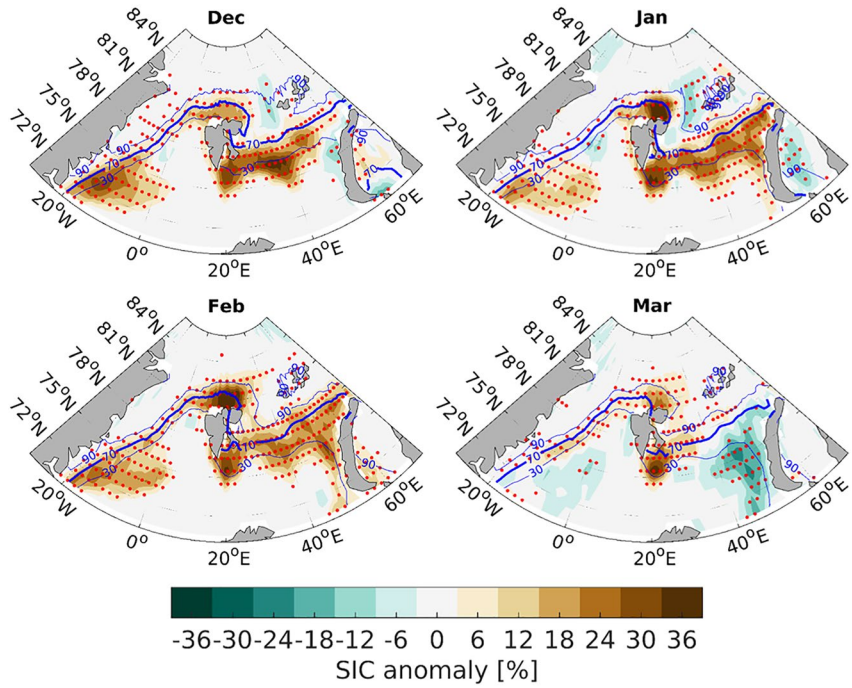

Figure 11. HadISST sea ice concentration composite anomalies for "marine cold air outbreaks (MCAO)" minus "low MCAO" conditions for December (top left), January (top right), February (bottom left), and March (bottom right). See Section 3.3 for more details on the compositing procedure. Red dots indicate grid boxes of statistically significant (95%) anomalies. See Section 3.3 for more details on the compositing procedure. Also shown is the HadISST climatological monthly mean sea ice concentration (blue contours).

has been increasingly ice-free in recent winters (Onarheim et al., 2014). This is plausible given the northerly wind (Figure 4) and cold (Figure 6) anomalies that are associated with MCAOs on Svalbard. There are also positive SIC anomalies evident along much of the climatological sea ice edge in Fram Strait, which translates to a southward shift of the latter during MCAOs. A striking feature is that MCAOs are related to significant positive SIC anomalies in the Barents Sea marginal ice zone during December, January and February, but not in March. In March, MCAOs are rather associated with negative SIC anomalies in the eastern Barents Sea. This seasonally changing connection between Fram Strait MCAOs and Barents Sea SIC is not straight-forward, so we analyzed atmospheric circulation patterns that are associated with SIC anomalies in the northern Barents Sea. SIC is affected by multiple processes, but large-scale atmospheric forcing plays an important role. For instance, SIC is affected by wind-driven sea ice drift and convergence/divergence, as well as by manipulating freezing/thawing through radiative and thermodynamic forcing as consequence of certain weather regimes. Figure 12 shows MSLP composite maps for "low ice" minus "high ice" conditions area-averaged in the displayed box (30°E–60°E, 74°N–79°N). We note that the following results are robust to reasonably small variations in the selected box that covers the Barents Sea marginal ice zone (not shown). In all displayed months, lower SIC in the region is paralleled by anomalous southerly flow over the Barents Sea as indicated by the isobars, consistent with the advection of comparably warm and moist air from the open water areas in the south. Apart from that, there are some interesting differences between the months. From December to February, anomalous high pressure is indicated over Novaya Zemlya and the eastern Barents Sea. This bears resemblance to the Arctic dipole anomaly (Wu et al., 2006) and the Scandinavian (Crasemann et al., 2017) - or Ural blocking (Cho & Kim, 2021), and all three studies linked this atmospheric constellation to sea ice loss in the Barents/Kara Seas, consistent with our results. It should be emphasized that the SIC compositing has been applied to detrended time series to avoid simply reproducing the large overarching trends. For example, the averge "low sea ice" year in the December composite is 2000.4 and the average "high sea ice" December is 1999.2. January additionally shows widespread cyclonic anomalies over the Greenland Sea and Svalbard. This reflects the negative effect on SIC by southerly advection in the eastern flank of cyclones passing over Fram Strait. The reason why MCAOs are associated with positive Barents Sea SIC anomalies from December to February emerges from comparing Figures 4 and 12. MCAOs

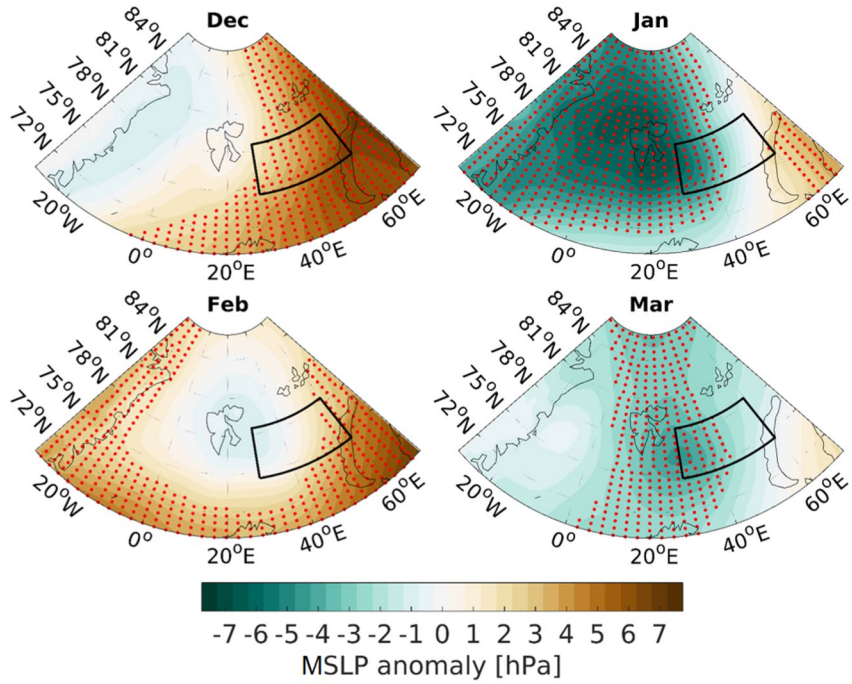

Figure 12. Mean sea level pressure (MSLP) composite anomalies for "sea ice concentration (SIC)" minus "high SIC" conditions in the Barents Sea (area-averaged in the displayed box covering 30°E–60°E, 74°N–79°N) for December (top left), January (top right), February (bottom left), and March (bottom right). Red dots indicate grid boxes of statistically significant (95%) anomalies. See Section 3.3 for more details on the compositing procedure.

relate to the dipole of anomalous low pressure over the eastern Barents Sea and anomalous high pressure over the Greenland Sea (Figure 4), while the approximate opposite pattern is found for low minus high sea ice conditions. In other words, the meridional flow regime which drives SIC reductions in the Barents Sea from December to February cannot be reconciled with the MCAO-related Barents Sea low pressure anomaly.

The MSLP composite pattern for March differs from the other months, since it consists of a low pressure anomaly that is confined to the western Barents Sea and extends well into the central Arctic. This low pressure anomaly could reflect cyclones migrating to that region, or a locally forced low pressure anomaly over an area of reduced sea ice cover. The latter can be explained by increased heat fluxes over anomalous open water areas, which warm and moisten the atmospheric boundary layer and give rise to enhanced baroclinicity. These mechanisms can in turn amplify baroclinic cyclones in the region of sea ice loss and enhance their persistence (Honda et al., 2009; Inoue & Hori, 2011; Rinke et al., 2017).

Barents Sea sea ice is in retreat during all the displayed months (Onarheim et al., 2018), but none of the associated circulation patterns during December, January or February in Figure 12 is consistent with an increased Fram Strait zonal pressure gradient and hence increased MCAOs. Only the Barents Sea low pressure anomaly during March relates to enhanced northerlies in Fram Strait and north of it, being consistent with enhanced Fram Strait MCAOs. These results provide a plausible explanation why the observed MCAO increase appears only during March, but more process-oriented studies would be needed to disentangle and quantify the involved relationships.

5. Discussion and Conclusions

We have conducted a systematic assessment of climatological intensities, and occurrence frequencies of different intensity classes of MCAOs in Fram Strait based on the last 42 years in the novel ERA5 reanalysis product. There is strong interannual variability in both MCAO intensities and occurrence frequencies, and overall MCAOs are evident around 2/3 of the time. Consistent with earlier studies (e.g., Kolstad et al., 2009; Mallet et al., 2013; Terpstra et al., 2021) we find that MCAOs are associated with a dipole-like circulation pattern in the lower troposphere, consisting of anomalously high pressure over Greenland, and anomalous low pressure over the

Barents/Kara Seas. Our results show that the magnitude of the dipole pattern and the related zonal pressure gradient over Fram Strait scales with the associated MCAO magnitude, suggesting a strong role of atmospheric dynamics in driving MCAO variability. February and March 2020 set new positive records for the monthly mean MCAO index in Fram Strait, and February moreover for the associated zonal pressure gradient. These features could be traced down to few individual MCAO events, including the strongest February event, and the second strongest March event on record. For the March event we apply a method proposed by Ali and Pithan (2020). Thereby, radiosonde observations from the MOSAiC expedition 2019/2020 in the central Arctic, located in the upstream direction of the MCAO advection event, are combined with corresponding observations in Ny-Ålesund, Svalbard, after the two locations have been dynamically matched by air back-trajectories during the peak MCAO phase. The results highlight the otherwise rarely observed diabatic cooling and drying in the MCAO preconditioning phase and we suggest that the methodology can be an insightful tool for dedicated studies on the vertical footprint of MCAO air mass transformations along the advection pathway.

The second part of the study investigates decadal MCAO trends and their drivers over the 1979–2020 period. While the bulk of existing MCAO studies consider multi-month averages over the extended winter season (e.g., Afargan-Gerstman et al., 2020; Mallet et al., 2013; Papritz & Grams, 2018; Papritz & Spengler, 2017), we are breaking down our analysis to individual months to highlight sub-seasonal changes. We find significant MCAO decreases in December and January that are consistent with the differing pace of warming between the surface and the lower atmosphere. On the other hand, a significant MCAO increase in March is revealed that can be explained dynamically with increased northerlies across Fram Strait as a result of a cyclonic circulation anomaly over the Barents/Kara Sea. In an attempt to explain the seasonal MCAO and circulation trends, we analyze the impact of the North Atlantic Oscillation (NAO), and sea ice concentration (SIC). The results suggest that the NAO has only very limited impact in agreement with Afargan-Gerstman et al. (2020). In March, a cyclonic circulation anomaly over the region of pronounced Barents Sea sea ice loss is identified, which feeds back on enhanced northerlies in Fram Strait. This finding for March is in contrast to the individual months earlier in the winter season (December through February), when low SIC conditions in the Barents Sea are rather associated with blocking high pressure regimes east of the SIC anomaly and/or cyclonic activity west of it (Cho & Kim, 2021; Crasemann et al., 2017; Wu et al., 2006). This could provide a possible explanation for the MCAO increase in March by sea ice – cyclone interactions in the Barents Sea. Further analysis is needed to disentangle whether enhanced cyclonic activity in the Barents Sea is a cause or an effect of sea ice reduction – both ways are plausible and likely affect each other. On the one hand side, reduced SIC enables baroclinic cyclones to intensify and to penetrate further into the Arctic (Honda et al., 2009; Inoue & Hori, 2011; Rinke et al., 2017; Valkonen et al., 2021). On the other hand side, baroclinic cyclones can drive sea ice reductions via dynamical wind forcing and by the amount of heat and moisture they carry toward the sea ice (Woods & Caballero, 2016). The nonlinear, complex nature of those relationships can be illustrated on the example of the 2020 MCAO season: Despite recordbreaking MCAOs in late winter/spring, SIC and sea ice thickness in the Barents Sea were anomalously high – a consequence of nonlinear thermodynamic and dynamic processes (Dethloff et al., 2021). There is also evidence that the polar stratosphere can modulate MCAOs. Afargan-Gerstman et al. (2020) identified a link between sudden stratospheric warmings (SSWs) and decreased MCAO occurrence in the Nordic Seas, while Papritz and Grams (2018) found that a strong (weak) polar vortex during winter can favor a strong (weak) MCAO season in Fram Strait. These links depend regionally on the degree to which stratospheric anomalies impact the occurrence of cyclonic and blocking weather regimes in the lower troposphere. For instance, polar vortex strength itself was shown to impact MCAOs mainly in the Greenland/Irminger Seas including Fram Strait (Papritz & Grams, 2018), while the effect of SSWs seems to be focused on Norwegian/Southern Barents Sea MCAOs. The link between stratospheric anomalies and MCAOs is particularly interesting and deserves further investigation, as the recordbreaking MCAO season 2020 coincided with a recordbreaking strong polar vortex (Lawrence et al., 2020), hence underlining the potential impact of the stratosphere on the 2020 MCAOs season.

As noted in Landgren et al. (2019), future projections of MCAOs are strongly shaped by the spatial pattern of sea ice edge retreat. Despite the widespread seasonal Arctic sea ice loss over the last decades, the sea ice edge position in Fram Strait has remained rather unchanged (Onarheim et al., 2014; Stroeve & Notz, 2018), particularly in March. Future sea ice retreat however could well manipulate Fram Strait MCAOs, in a manner comparable to what is already observed in Whalers Bay polynya north of Svalbard. For this region substantial recent sea ice loss has been reported (Onarheim et al., 2014), and Tetzlaff et al. (2014) showed that the newly available open water areas can drive MCAOs and convective boundary layers of intensities that were previously unknown to that

region. With an ongoing warming it cannot be ruled out that this will affect the conditions in Fram Strait and the related MCAO season.

Data Availability Statement

We acknowledge the use of imagery from the NASA Worldview application (https://worldview.earthdata.nasa.gov), part of the NASA Earth Observing System Data and Information System (EOSDIS). ECMWF is acknowledged for providing the ERA5 reanalysis data, which were downloaded in MARS and are publicly accessible via the Climate Data Store (CDS). The authors gratefully acknowledge the NOAA Air Resources Laboratory (ARL) for the provision of the HYSPLIT transport and dispersion model and READY website (https://www.ready.noaa.gov) used in this publication. The Ny-Ålesund radiosonde record is available under https://doi.org/10.1594/PANGAEA.914973. The radiosonde record of the MOSAiC expedition is available under https://doi.org/10.1594/PANGAEA.928656. HadISST data were obtained from https://www.metoffice.gov.uk/hadobs/hadisst/ and are © British Crown Copyright, Met Office, 2003, provided under a Non-Commercial Government License http://www.nationalarchives.gov.uk/doc/non-commercial-government-licence/version/2/.

Acknowledgments
We gratefully acknowledge the funding by the Deutsche Forschungsgemeinschaft (DFG, German Research Foundation) – project no. 268020496 – TRR 172, within the Transregional Collaborative Research Center "ArctiC Amplification: Climate Relevant Atmospheric and SurfaCe Processes, and Feedback Mechanisms (AC)3". Some data used in this paper were produced as part of RV Polarstern cruise AWI_PS121 and of the international Multidisciplinary drifting Observatory for the Study of the Arctic Climate (MOSAiC) with the tag MOSAiC20192020 (AWI_PS122_00). Radiosonde data were obtained through a partnership between the leading Alfred Wegener Institute (AWI), the atmospheric radiation measurement (ARM) user facility, a US Department of Energy facility managed by the Biological and Environmental Research Program, and the German Weather Service (DWD). S. Dahlke received support from the project "Quantifying Rapid Climate Change in the Arctic: regional feedbacks and large-scale impacts (QUARCCS)" funded by the German and Russian Ministries of Research and Education. Open access funding enabled and organized by Projekt DEAL.

References

Afargan-Gerstman, H., Polkova, I., Papritz, L., Ruggieri, P., King, M. P., Athanasiadis, P. J., et al. (2020). Stratospheric influence on North Atlantic marine cold air outbreaks following sudden stratospheric warming events. *Weather and Climate Dynamics*, *1*, 541–553. https://doi.org/10.5194/wcd-1-541-2020

Alfred-Wegener-Institut Helmholtz-Zentrum für Polar- und Meeresforschung. (2017). Polar research and supply vessel POLARSTERN operated by the Alfred-Wegener-Institute. *Journal of large-scale research facilities*, *3*, A119. https://doi.org/10.17815/jlsrf-3-163

Ali, S. M., & Pithan, F. (2020). Following moist intrusions into the Arctic using SHEBA observations in a Lagrangian perspective. *Quarterly Journal of the Royal Meteorological Society*, *146*, 3522–3533. https://doi.org/10.1002/qj.3859

Bracegirdle, T. J., & Gray, S. L. (2008). An objective climatology of the dynamical forcing of polar lows in the Nordic seas. *International Journal of Climatology*, *28*, 1903–1919. https://doi.org/10.1002/joc.1686

Brümmer, B. (1996). Boundary-layer modification in wintertime cold-air outbreaks from the Arctic sea ice. *Boundary-Layer Meteorology*, *80*, 109–125. https://doi.org/10.1007/BF00119014

Cho, D. J., & Kim, K. Y. (2021). Role of Ural blocking in Arctic sea ice loss and its connection with Arctic warming in winter. *Climate Dynamics*, *56*, 1571–1588. https://doi.org/10.1007/s00382-020-05545-3

Cokelet, E. D., Tervalon, N., & Bellingham, J. G. (2008). Hydrography of the West Spitsbergen current, Svalbard branch: Autumn 2001. *Journal of Geophysical Research*, *113*, C01006. https://doi.org/10.1029/2007JC004150

Crasemann, B., Handorf, D., Jaiser, R., Dethloff, K., Nakamura, T., Ukita, J., & Yamazaki, K. (2017). Can preferred atmospheric circulation patterns over the North-Atlantic-Eurasian region be associated with arctic sea ice loss? *Polar Scienece*, *14*, 9–20. https://doi.org/10.1016/j.polar.2017.09.002

Dahlke, S., Hughes, N. E., Wagner, P. M., Gerland, S., Wawrzyniak, T., Ivanov, B., & Maturilli, M. (2020). The observed recent surface air temperature development across Svalbard and concurring footprints in local sea ice cover. *International Journal of Climatology*, *40*, 5246–5265. https://doi.org/10.1002/joc.6517

Dahlke, S., & Maturilli, M. (2017). Contribution of atmospheric advection to the Amplified winter warming in the Arctic North Atlantic region. *Advances in Meteorology*, *2017*, 8. https://doi.org/10.1155/2017/4928620

Dethloff, K., Maslowski, W., Hendricks, S., Lee, Y., Goessling, H. F., Krumpen, T., et al. (2021). Arctic sea ice anomalies during the MOSAiC winter 2019/2020 [Preprint]. The Cryosphere Discuss, https://doi.org/10.5194/tc-2020-375

Dickson, R., Lazier, J., Meincke, J., Rhines, P., & Swift, J. (1996). Long-term coordinated changes in the convective activity of the North Atlantic. *Progress in Oceanography*, *38*, 241–295. https://doi.org/10.1016/S0079-6611(97)00002-5

Duarte, P., Sundfjord, A., Meyer, A., Hudson, S. R., Spreen, G., & Smedsrud, L. H. (2020). Warm Atlantic water explains observed sea ice melt rates north of Svalbard. *Journal of Geophysical Research: Oceans*, *125*, e2019JC015662. https://doi.org/10.1029/2019JC015662

Graham, R. M., Cohen, L., Ritzhaupt, N., Segger, B., Graversen, R. G., Rinke, A., et al. (2019). Evaluation of six atmospheric reanalyses over Arctic sea ice from winter to early summer. *Journal of Climate*, *32*(14), 4121–4143. https://doi.org/10.1175/JCLI-D-18-0643.1

Graham, R. M., Hudson, S. R., & Maturilli, M. (2019). Improved performance of ERA5 in Arctic gateway relative to four global atmospheric reanalyses. *Geophysical Research Letters*, *46*, 6138–6147. https://doi.org/10.1029/2019GL082781

Graversen, R., Mauritsen, T., Tjernström, M., Källén, E., & Svensson, G. (2008). Vertical structure of recent Arctic warming. *Nature*, *451*, 53–56. https://doi.org/10.1038/nature06502

Hersbach, H., Bell, B., Berrisford, P., Hirahara, S., Horányi, A., Muñoz-Sabater, J., et al. (2020). The ERA5 global reanalysis. *Quarterly Journal of the Royal Meteorological Society*, *146*, 1999–2049. https://doi.org/10.1002/qj.3803

Honda, M., Inoue, J., & Yamane, S. (2009). Influence of low Arctic sea-ice minima on anomalously cold Eurasian winters. *Geophysical Research Letters*, *36*, L08707. https://doi.org/10.1029/2008GL037079

Hurrell, J. W., Kushnir, Y., Ottersen, G., & Visbeck, M. (2003). An overview of the North Atlantic oscillation. In J. W. Hurrell, Y. Kushnir, G. Ottersen, & M. Visbeck (Eds.), *The North Atlantic oscillation: Climatic significance and environmental impact* (pp. 1–35). American Geophysical Union (AGU). https://doi.org/10.1029/134GM01

Hyland, R., & Wexler, A. (1983). Formulations for the thermodynamic properties of the saturated phases of H_2O from 173.15 K to 473.15 K. *ASHRAE Transactions*, *89*(2A), 500–519.

Inoue, J., & Hori, M. E. (2011). Arctic cyclogenesis at the marginal ice zone: A contributory mechanism for the temperature amplification. *Geophysical Research Letters*, *38*, L12502. https://doi.org/10.1029/2011GL047696

Isachsen, P. E., Drivdal, M., Eastwood, S., Gusdal, Y., Noer, G., & Saetra, Ø. (2013). Observations of the ocean response to cold air outbreaks and polar lows over the Nordic Seas. *Geophysical Research Letters*, *40*, 3667–3671. https://doi.org/10.1002/grl.50705

Kanno, Y., Abdillah, M. R., & Iwasaki, T. (2015). Charge and discharge of polar cold air mass in northern hemispheric winter. *Geophysical Research Letters*, *42*, 7187–7193. https://doi.org/10.1002/2015GL065626

Kendall, M. G. (1975). *Rank correlation methods* (4th ed.). Charles Griffin.

Kim, B.-M., Hong, J.-Y., Jun, S.-Y., Kwon, H., Kim, S.-J., & Kim, J.-H. (2017). Major cause of unprecedented Arctic warming in January 2016: Critical role of an Atlantic windstorm. *Scientific Reports*, *7*, 40051. https://doi.org/10.1038/srep40051

Knudsen, E. M., Heinold, B., Dahlke, S., Bozem, H., Crewell, S., Gorodetskaya, I. V., et al. (2018). Meteorological conditions during the ACLOUD/PASCAL field campaign near Svalbard in early summer 2017. *Atmospheric Chemistry and Physics*, *18*, 17995–18022. https://doi.org/10.5194/acp-18-17995-2018

Kolstad, E. W. (2017). Higher ocean wind speeds during marine cold air outbreaks. *Quarterly Journal of the Royal Meteorological Society*, *143*, 2084–2092. https://doi.org/10.1002/qj.3068

Kolstad, E. W., & Bracegirdle, T. J. (2008). Marine cold-air outbreaks in the future: An assessment of IPCC AR4 model results for the northern hemisphere. *Climate Dynamics*, *30*, 871–885. https://doi.org/10.1007/s00382-007-0331-0

Kolstad, E. W., Bracegirdle, T. J., & Seierstad, I. A. (2009). Marine cold-air outbreaks in the North Atlantic: Temporal distribution and associations with large-scale atmospheric circulation. *Climate Dynamics*, *33*, 187–197. https://doi.org/10.1007/s00382-008-0431-5

Landgren, O. A., Seierstad, I. A., & Iversen, T. (2019). Projected future changes in marine cold-air outbreaks associated with polar lows in the northern North-Atlantic ocean. *Climate Dynamics*, *53*, 2573–2585. https://doi.org/10.1007/s00382-019-04642-2

Lawrence, Z. D., Perlwitz, J., Butler, A. H., Manney, G. L., Newman, P. A., Lee, S. H., & Nash, E. R. (2020). The remarkably strong Arctic stratospheric polar vortex of winter 2020: Links to record-breaking Arctic oscillation and ozone loss. *Journal of Geophysical Research: Atmospheres*, *125*, e2020JD033271. https://doi.org/10.1029/2020JD033271

Mallet, P.-E., Claud, C., Cassou, C., Noer, G., & Kodera, K. (2013). Polar lows over the Nordic and Labrador Seas: Synoptic circulation patterns and associations with North Atlantic-Europe wintertime weather regimes. *Journal of Geophysical Research: Atmospheres*, *118*, 2455–2472. https://doi.org/10.1002/jgrd.50246

Mann, H. B. (1945). Nonparametric tests against trend. *Econometrica*, *13*(3), 245–259. https://doi.org/10.2307/1907187

Maturilli, M. (2020). High resolution radiosonde measurements from station Ny-Ålesund (2017-04 et seq). Alfred Wegener Institute - Research Unit Potsdam, PANGAEA. https://doi.org/10.1594/PANGAEA.914973

Maturilli, M., Holdridge, D. J., Dahlke, S., Graeser, J., Sommerfeld, A., Jaiser, R., et al. (2021). *Initial radiosonde data from 2019-10 to 2020-09 during project MOSAiC*. Alfred Wegener Institute, Helmholtz Centre for Polar and Marine Research. https://doi.org/10.1594/PANGAEA.928656

Maturilli, M., & Kayser, M. (2017). Arctic warming, moisture increase and circulation changes observed in the Ny-Ålesund homogenized radiosonde record. *Theoretical and Applied Climatology*, *130*, 1–17. https://doi.org/10.1007/s00704-016-1864-0

Messori, G., Woods, C., & Caballero, R. (2018). On the drivers of wintertime temperature extremes in the high Arctic. *Journal of Climate*, *31*(4), 1597–1618. https://doi.org/10.1175/JCLI-D-17-0386.1

Meyer, M., Polkova, I., Modali, K. R., Schaffer, L., Baehr, J., Olbrich, S., & Rautenhaus, M. (2021). Interactive 3-D visual analysis of ERA5 data: Improving diagnostic indices for marine cold air outbreaks and polar lows. *Weather and Climate Dynamics*, *2*, 867–891. https://doi.org/10.5194/wcd-2-867-2021

Onarheim, I. H., Eldevik, T., Smedsrud, L. H., & Stroeve, J. C. (2018). Seasonal and regional manifestation of Arctic sea ice loss. *Journal of Climate*, *31*(12), 4917–4932. https://doi.org/10.1175/JCLI-D-17-0427.1

Onarheim, I. H., Smedsrud, L. H., Ingvaldsen, R. B., & Nilsen, F. (2014). Loss of sea ice during winter north of Svalbard. *Tellus A: Dynamic Meteorology and Oceanography*, *66*(1). https://doi.org/10.3402/tellusa.v66.23933

Overland, J. E., & Wang, M. (2021). The 2020 Siberian heat wave. *International Journal of Climatology*, *41*(1), E2341–E2346. https://doi.org/10.1002/joc.6850

Papritz, L. (2020). Arctic lower-tropospheric warm and cold extremes: Horizontal and vertical transport, diabatic processes, and linkage to synoptic circulation features. *Journal of Climate*, *33*(3), 993–1016. https://doi.org/10.1175/JCLI-D-19-0638.1

Papritz, L., & Grams, C. M. (2018). Linking low-frequency large-scale circulation patterns to cold air outbreak formation in the northeastern North Atlantic. *Geophysical Research Letters*, *45*, 2542–2553. https://doi.org/10.1002/2017GL076921

Papritz, L., Rouges, E., Aemisegger, F., & Wernli, H. (2019). On the thermodynamic preconditioning of Arctic air masses and the role of tropopause polar vortices for cold air outbreaks from Fram Strait. *Journal of Geophysical Research: Atmospheres*, *124*, 11033–11050. https://doi.org/10.1029/2019JD030570

Papritz, L., & Spengler, T. (2017). A Lagrangian climatology of wintertime cold air outbreaks in the Irminger and Nordic seas and their role in shaping air–sea heat fluxes. *Journal of Climate*, *30*(8), 2717–2737. https://doi.org/10.1175/jcli-d-16-0605.1

Pithan, F., Svensson, G., Caballero, R., Chechin, D., Cronin, T. W., Ekman, A. M. L., et al. (2018). Role of air-mass transformations in exchange between the Arctic and mid-latitudes. *Nature Geoscience*, *11*, 805–812. https://doi.org/10.1038/s41561-018-0234-1

Polkova, I., Afargan-Gerstman, H., Domeisen, D. I. V., King, M. P., Ruggieri, P., Athanasiadis, P., et al. (2021). Predictors and prediction skill for marine cold-air outbreaks over the Barents Sea. *Quarterly Journal of the Royal Meteorological Society*, *147*, 2638–2656. https://doi.org/10.1002/qj.4038

Rayner, N. A., Parker, D. E., Horton, E. B., Folland, C. K., Alexander, L. V., Rowell, D. P., et al. (2003). Global analyses of sea surface temperature, sea ice, and night marine air temperature since the late nineteenth century. *Journal of Geophysical Research: Atmospheres*, *108*(D14), 4407. https://doi.org/10.1029/2002JD002670

Rinke, A., Maturilli, M., Graham, R. M., Matthes, H., Handorf, D., Cohen, L., et al. (2017). Extreme cyclone events in the Arctic: Wintertime variability and trends. *Environmental Research Letters*, *12*(9), 094006. https://doi.org/10.1088/1748-9326/aa7def

Rolph, G., Stein, A., & Stunder, B. (2017). Real-time environmental applications and display system: Ready. *Environmental Modelling & Software*, *95*, 210–228. https://doi.org/10.1016/j.envsoft.2017.06.025

Rydsaa, J. H., Graversen, R. G., Heiskanen, T. I. H., & Stoll, P. J. (2021). Changes in atmospheric latent energy transport into the Arctic: Planetary versus synoptic scales. *Quarterly Journal of the Royal Meteorological Society*, *147*, 2281–2292. https://doi.org/10.1002/qj.4022

Sen, P. K. (1968). Estimates of the regression coefficient based on Kendall's tau. *Journal of the American Statistical Association*, *63*(324), 1379–1389. https://doi.org/10.1080/01621459.1968.10480934

Serreze, M. C., Barrett, A. P., & Cassano, J. J. (2011). Circulation and surface controls on the lower tropospheric air temperature field of the Arctic. *Journal of Geophysical Research*, *116*, D07104. https://doi.org/10.1029/2010JD015127

Serreze, M. C., Barrett, A. P., Stroeve, J. C., Kindig, D. N., & Holland, M. M. (2009). The emergence of surface-based Arctic amplification. *The Cryosphere*, *3*, 11–19. https://doi.org/10.5194/tc-3-11-2009

Shupe, M. D., Rex, M., Dethloff, K., Damm, E., Fong, A. A., Gradinger, R., et al. (2020). The MOSAiC expedition: A year drifting with the Arctic sea ice. *Arctic Report Card*. https://doi.org/10.25923/9g3v-xh92

Stein, A. F., Draxler, R. R., Rolph, G. D., Stunder, B. J. B., Cohen, M. D., & Ngan, F. (2015). NOAA's HYSPLIT atmospheric transport and dispersion modeling system. *Bulletin of the American Meteorological Society*, *96*, 2059–2077. https://doi.org/10.1175/BAMS-D-14-00110.1

Stoll, P. J., Graversen, R. G., Noer, G., & Hodges, K. (2018). An objective global climatology of polar lows based on reanalysis data. *Quarterly Journal of the Royal Meteorological Society*, *144*, 2099–2117. https://doi.org/10.1002/qj.3309

Stroeve, J., & Notz, D. (2018). Changing state of Arctic sea ice across all seasons. *Environmental Research Letters*, *13*, 103001. https://doi.org/10.1088/1748-9326/aade56

Terpstra, A., Renfrew, I. A., & Sergeev, D. E. (2021). Characteristics of cold-air outbreak events and associated polar mesoscale cyclogenesis over the North Atlantic region. *Journal of Climate*, *34*(11), 4567–4584. https://doi.org/10.1175/JCLI-D-20-0595.1

Tetzlaff, A., Lüpkes, C., Birnbaum, G., Hartmann, J., Nygård, T., & Vihma, T. (2014). Brief Communication: Trends in sea ice extent north of Svalbard and its impact on cold air outbreaks as observed in spring 2013. *The Cryosphere*, *8*, 1757–1762. https://doi.org/10.5194/tc-8-1757-2014

Theil, H. (1950). A rank-invariant method of linear and polynominal regression analysis (parts 1–3). *Nederlandse Akademie van Wetenschappen Proceedings Series A*, *53*, 1397–1412.

Valkonen, E., Cassano, J., & Cassano, E. (2021). Arctic cyclones and their interactions with the declining sea ice: A recent climatology. *Journal of Geophysical Research: Atmospheres*, *126*, e2020JD034366. https://doi.org/10.1029/2020JD034366

Vavrus, S., Walsh, J. E., Chapman, W. L., & Portis, D. (2006). The behavior of extreme cold air outbreaks under greenhouse warming. *International Journal of Climatology*, *26*, 1133–1147. https://doi.org/10.1002/joc.1301

Walczowski, W., & Piechura, J. (2011). Influence of the West Spitsbergen current on the local climate. *International Journal of Climatology*, *31*, 1088–1093. https://doi.org/10.1002/joc.2338

Wang, C., Graham, R. M., Wang, K., Gerland, S., & Granskog, M. A. (2019). Comparison of ERA5 and ERA-Interim near-surface air temperature, snowfall and precipitation over Arctic sea ice: Effects on sea ice thermodynamics and evolution. *The Cryosphere*, *13*, 1661–1679. https://doi.org/10.5194/tc-13-1661-2019

Winther, J.-G., Godtliebsen, F., Gerland, S., & Isachsen, P. E. (2002). Surface albedo in Ny-Ålesund, Svalbard: Variability and trends during 1981–1997. *Global and Planetary Change*, *32*(2–3), 127–139. https://doi.org/10.1016/S0921-8181(01)00103-5

Woods, C., & Caballero, R. (2016). The role of moist intrusions in winter Arctic warming and sea ice decline. *Journal of Climate*, *29*(12), 4473–4485. https://doi.org/10.1175/JCLI-D-15-0773.1

Wu, B., Wang, J., & Walsh, J. E. (2006). Dipole anomaly in the winter Arctic atmosphere and its association with sea ice motion. *Journal of Climate*, *19*(2), 210–225. https://doi.org/10.1175/JCLI3619.1

Yue, S., Pilon, P., Phinney, B., & Cavadias, G. (2002). The influence of autocorrelation on the ability to detect trend in hydrological series. *Hydrological Processes*, *16*, 1807–1829. https://doi.org/10.1002/hyp.1095